

高まることが観察された。しかしながら、変異の種類によってはその効果が十分ではなく、この点を改善するような新たな siRNA の化学修飾などを今後検討しなければならないと考える。

E. 結論

ホタル、ウミシイタケ・ルシフェラーゼレポーター遺伝子をリポーターアレルとして、アレル特異的 RNAi 効果を評価するシステムの確立を行った。確立したシステムは、従来の方法では解析が不可能であった正常型/変異型アレルがヘテロで存在する条件下で、変異アレルに対する RNAi 発現抑制効果と正常アレルに与える影響を同時に評価することができる。

F. 研究発表

1. 論文発表

- 1) Ohnishi Y., Tokunaga K., Hohjoh H.: Influence of assembly of siRNA elements into RNA-induced silencing complex (RISC) by fork-siRNA duplex carrying nucleotide mismatches at the 3'- or 5'-end of the sense-stranded siRNA element. *BBRC*, 329: 516-521, 2005
- 2) Tamura Y., Sakasegawa Y., Omi K., Kishida H., Asada T., Kimura H., Tokunaga K., Hachiya N.S., Kaneko K., Hohjoh H.: Association study of the chemokine, CXC motif, ligand 1 (CXCL1) gene with sporadic Alzheimer's disease in a Japanese population. *Neurosci. Letters*, 379: 149-151, 2005

2. 学会発表

- 1) Ohnishi Y., Tokunaga K., Kaneko K., and Hohjoh H. (2005) "Evaluation system for siRNA duplexes conferring allele-specific

gene silencing." 55th Annual Meeting of the American Society of Human Genetics, Salt Lake City, Utah, USA.

- 2) Kawashima M., Tamiya G., Hohjoh H., Juji T., Ebisawa T., Honda Y., Inoko H., Tokunaga K. (2005) "A new resistant gene candidate for human narcolepsy identified by a genome-wide association study" 55th Annual Meeting of the American Society of Human Genetics, Salt Lake City, Utah, USA.
- 3) 田村美子、功刀浩、金子清俊、北條浩彦. (2005) 「ヒト RELN 遺伝子の DNA メチル化と遺伝子発現レベルの解析」第 28 回日本分子生物学会、福岡.
- 4) 大西悠亮、徳永勝士、徳永勝士、金子清俊、北條浩彦. (2005) 「対立遺伝子特異的 RNAi 効果をヘテロ接合体下で評価するアッセイ系の確立」第 28 回日本分子生物学会、福岡.
- 5) 山本真央、高須美和、徳永勝士、数藤由美子、平井百樹、北條浩彦、功刀浩、上野美華子、南光進一郎. (2005) 「均衡型染色体転座部位における双極性障害疾患感受性遺伝子探索」第 28 回日本分子生物学会、福岡.

G. 知的財産権の出願・登録状況

特許出願番号：2005-116177

発明者：北條浩彦

発明の名称：「対立遺伝子に対する特異的 RNAi の評価方法」

出願人：財団法人ヒューマンサイエンス振興財団とプロメガ株式会社との共同出願

出願日：平成 17 年 4 月 13 日

研究成果の刊行に関する一覧表

書籍

著者氏名	論文タイトル名	書籍全体の編集者名	書籍名	出版社名	出版地	出版年	ページ
Hachiya NS, Kaneko K	Investigation of laser microdissected inclusion bodies	Berns M, Greulich KO	Method in Cell Biology	Academic Press	New York	2006	In press
K.Kuwata.	Semi-classical quantization of protein dynamics:Novel NMR relaxation formalism and its application to prion.	T.Kitamoto	PRIONS- Food and Drug Safety.	Springer-Verlag Tokyo	Tokyo	2005	155-170
八谷如美, 金子清俊	プリオン病の治療-現状と将来展望-	柳沢信夫, 篠原幸人, 岩田誠, 清水輝夫, 寺本明	Annual Review2005 神経	中外医学社	東京	2006	90-95
金子清俊	不思議なプリオン病	井原康夫	脳はどこまでわかったか. 朝日選書 771	朝日新聞社	東京	2005	771-
金子清俊	プリオン病.	三木哲郎	日常診療に活かす老年病ガイドブック-認知症・うつ・睡眠障害の診療の実際-	Medical View	東京	2005	173-179
桑田一夫	プリオンタンパク質	後藤祐児, 桑島邦博, 谷澤克行	タンパク質科学 - 構造・物性・機能 -	化学同人	京都	2005	315-330

雑誌

発表者氏名	論文タイトル名	発表誌名	巻号	ページ	出版年
Hachiya NS, Yamada M, Watanabe K, Jozuka A, Ohkubo T, Sano K, Takeuchi Y, Kozuka Y, Sakasegawa Y, Kaneko K	Mitochondrial localization of cellular prion protein (PrP ^C) invokes neuronal apoptosis in aged transgenic mice overexpressing PrP ^C	Neurosci Lett	74	98-103	2005
Hachiya NS, Watanabe K, Kawabata MY, Jozuka A, Ohkubo T, Kozuka Y, Sakasegawa Y, Kaneko K	Prion protein with Y145STOP mutation induces mitochondria-mediated apoptosis and PrP-containing deposits in vitro	Biochem Biophys Res Commun	327	894-899	2005

発表者氏名	論文タイトル名	発表誌名	巻号	ページ	出版年
Tamura Y, Sakasegawa Y, Omi K, Kishida H, Asada T, Kimura H, Tokunaga K, Hachiya NS, Kaneko K, Hohjoh H	Association study of the chemokine, CXC motif, ligand 1 (CXCL1) gene with sporadic Alzheimer's disease in a Japanese population	Neurosci Lett	379	149-151	2005
Noma T, Ikebukuro K, Sode K, Ohkubo T, Sakasegawa Y, Hachiya NS, Kaneko K	Screening of DNA aptamers against multiple proteins in tissue	Nucleic Acids Symposium Series	49	357-358	2005
Omi K, Hachiya NS, Tokunaga K, Kaneko K	siRNA-mediated inhibition of endogenous Huntington disease gene expression induces an aberrant configuration of the ER network <i>in vitro</i>	Biochem Biophys Res Commun	338	1229-1235	2005
Kaneko K, Hachiya NS	Hypothesis: Gut as source of motor neuron toxin in the development of ALS	Med Hypotheses	66	438-439	2006
Ohkubo T, Sakasegawa Y, Toda H, Kishida H, Arima K, Yamada M, Takahashi H, Mizusawa H, Hachiya NS, Kaneko K	Three-repeat tau 69 is a major tau isoform in laser-microdissected pick bodies	Amyloid		In press	2006
Kaneko K, Hachiya NS	The alternative role of 14-3-3 zeta as a sweeper of misfolded proteins in disease conditions	Med Hypotheses		In press	2006
Soeda A, Nakashima T, Okumura A, Kuwata K, Shinoda J, Iwama T.	Cognitive impairment after traumatic brain injury-a functional magnetic resonance imaging study using the Stroop task.	Neuroradiology	47(7)	501-506	2005

発表者氏名	論文タイトル名	発表誌名	巻号	ページ	出版年
Hashimoto K, Kato Z, Nagase T, Shimozawa N, Kuwata K, Omoya K, Li A, Matsukuma E, Yamamoto Y, Ohnishi H, Tochio H, Shirakawa M, Suzuki Y, Wanders RJ, Kondo N.	Molecular Mechanism of a Temperature-Sensitive Phenotype in Peroxisomal Biogenesis Disorder.	Pediatric Research.	58(2)	263-269	2005
Ohnishi Y, Tokunaga K, Hohjoh H	Influence of assembly of siRNA elements into RNA-induced silencing complex (RISC) by fork- siRNA duplex carrying nucleotide mismatches at the 3'- or 5'-end of the sense-stranded siRNA element	Biochem Biophys Res Commun	329	516-521	2005
Tamura Y, Sakasegawa Y, Omi K, Kishida H, Asada T, Kimura H, Tokunaga K, Hachiya NS, Kaneko K, Hohjoh H	Association study of the chemokine, CXC motif, ligand 1 (CXCL1) gene with sporadic Alzheimer's disease in a Japanese population.	Neurosci. Letters	379	149-151	2005

発表者氏名	論文タイトル名	発表誌名	巻号	ページ	出版年
金子清俊	クロイツフェルト・ヤコブ病	臨床と微生物	32	69-72	2005
八谷如美, 金子清俊	新しいシャペロンの発見 - 神経難病の治療へ -	科学	75	283-285	2005
八谷如美, 金子清俊	プリオン研究の進展	VIRUS REPORT	2	14-19	2005
金子清俊	vCJD (変異型クロイツフェルト・ヤコブ病)	日本評論社「からだの科学」	244	95	2005
金子清俊	BSE と食の安全	日本薬剤師会雑誌	57	81-84	2005
金子清俊	科学と行政 - 科学者と BSE 対策 -	現代化学	416	60-63	2005
八谷如美, 金子清俊	プリオン病の現状-牛海綿状脳症と変異型 CJD を中心に-	LABIO 21	22	5-10	2005
八谷如美, 金子清俊	牛海綿状脳症 (BSE) と変異型 CJD	Bios.	10	7-8	2005
金子清俊	特集「プリオン病」	医学のあゆみ	215	875	2005
八谷如美	特集「プリオン病」	医学のあゆみ	215		2005
金子清俊	理系の説明責任. BSE 問題をめぐって	科学	76	52-55	2005
八谷如美, 金子清俊	プリオン蛋白質異常化の分子機構	化学療法の領域	22	63-68	2006
金子清俊	牛海綿状脳症と変異型クロイツフェルト・ヤコブ病	TMDC MATE		印刷中	2005
金子清俊	プリオン病- 牛海綿状脳症 (BSE)と変異型クロイツフェルト・ヤコブ病	BRAIN		印刷中	2005
桑田一夫	バイオインフォマティクスによるプリオン病治療薬の開発	化学療法の領域	22	87-93	2006

Prion protein with Y145STOP mutation induces mitochondria-mediated apoptosis and PrP-containing deposits in vitro

Naomi S. Hachiya^{a,b}, Kota Watanabe^{a,b}, Makiko Y. Kawabata^{a,b}, Akiko Jozuka^{a,b},
Yoshimichi Kozuka^c, Yuji Sakasegawa^a, Kiyotoshi Kaneko^{a,b,*}

^a Department of Cortical Function Disorders, National Institute of Neuroscience (NIN), National Center of Neurology and Psychiatry (NCNP), Kodaira, Tokyo 187-8502, Japan

^b Core Research for Evolutional Science and Technology (CREST), Japan Science and Technology Corporation, Japan

^c Department of Ultrastructural Research, National Institute of Neuroscience (NIN), National Center of Neurology and Psychiatry (NCNP), Kodaira, Tokyo 187-8502, Japan

Received 2 December 2004

Available online 29 December 2004

Abstract

A pathogenic truncation of an amber mutation at codon 145 (Y145STOP) in Gerstmann–Straussler–Scheinker disease (GSS) was investigated through the real-time imaging in living cells, by utilizing GFP-PrP constructs. GFP-PrP(1–144) exhibited an aberrant localization to mitochondria in mouse neuroblastoma neuro2a (N2a) and HpL3-4 cells, a hippocampal cell line established from *prnp* gene-ablated mice, whereas full-length GFP-PrP did not. The aberrant mitochondrial localization was also confirmed by Western blot analysis. Since GFP-PrP(1–121), as previously reported, and full-length GFP-PrP do not exhibit such mitochondrial localization, the mitochondrial localization of GFP-PrP(1–144) requires not only PrP residues 121–144 (in human sequence) but also COOH-terminal truncation in the current experimental condition. Subsequently, the GFP-PrP(1–144) induced a change in the mitochondrial innermembrane potential ($\Delta\Psi_m$), release of cytochrome *c* from the intermembrane space into the cytosol, and DNA fragmentation in these cells. Non-fluorescent PrP(1–144) also induced the DNA fragmentation in N2a and HpL3-4 cells after the proteasomal inhibition. These data may provide clues as to the molecular mechanism of the neurotoxic property of Y145STOP mutation. Furthermore, immunoelectron microscopy revealed numerous electron-dense deposits in mitochondria clusters of GFP-PrP(1–144)-transfected N2a cells, whereas no deposit was detected in the cells transfected with full-length GFP-PrP. Co-localization of GFP/PrP-immunogold particles with porin-immunogold particles as a mitochondrial marker was observed in such electron-dense vesicular foci, resembling those found in autophagic vacuoles forming secondary lysosomes. Whether such electron-dense deposits may serve as a seed for the growth of amyloid plaques, a characteristic feature of GSS with Y145STOP, awaits further investigations.

© 2004 Elsevier Inc. All rights reserved.

Keywords: Cellular prion protein; Green fluorescent protein; PrP Y145STOP mutation; Mitochondria-mediated apoptosis; PrP-containing deposits

Prion protein (PrP) consists of two isoforms, one is a host-encoded cellular isoform (PrP^C) and the other is an abnormal protease-resistant pathogenic isoform (PrP^{Sc}), of which the latter is a causative agent of prion disease.

PrP^{Sc} stimulates the conversion of PrP^C into nascent PrP^{Sc}, and the accumulation of PrP^{Sc} leads to central nervous system dysfunction and neuronal degeneration both in humans and animals [1]. The human prion diseases include kuru, Creutzfeldt–Jakob disease, Gerstmann–Straussler–Scheinker disease (GSS), and fatal familial insomnia [2,3].

* Corresponding author. Fax: +81 42 346 1748.

E-mail address: kaneko@ncnp.go.jp (K. Kaneko).

We previously demonstrated the microtubule-associated intracellular localization of the NH₂-terminal fluorescent PrP^C fragment [4] in mouse neuroblastoma neuro2a (N2a) and HpL3-4 cells, a hippocampal cell line established from *prnp* gene-ablated mice [5], by utilizing double-labeled PrP^C. We detected NH₂-terminally fluorescent-tagged PrP^C predominantly in the intracellular compartments, COOH-terminally fluorescent-tagged PrP^C mostly at the cell surface membranes overlapping with lipid rafts, and PrP^C in full length with the merged color in Golgi compartments. Truncated PrP^C with the amino acid residues 1–121, 1–111, and 1–91 in mouse PrP exhibited a proper distribution profile. Following real-time imaging analysis with GFP-PrP^C revealed that the discrete NH₂-terminal amino acid residues are indispensable for the anterograde and the retrograde intracellular movements of GFP-PrP^C [6]. Consistent with our reports, other groups also found the GFP-tagged version of PrP^C to be properly anchored at the cell surface and its distribution pattern to be similar to that of the endogenous PrP^C, with labeling at the plasma membrane and in an intracellular perinuclear compartment [7–11].

Meanwhile, a pathogenic truncation of an amber mutation at codon 145 (Y145STOP) in the *prnp* gene, which was identified in a Japanese patient with GSS [12], came to our notice. The Y145STOP in human *prnp* gene corresponds to Y144STOP in mouse *prnp* gene which yields a product, mouse PrP(1–143) but hereafter designated PrP(1–144), and results in intracellular accumulation if proteasomal degradation is impaired [13]. Until now, its precise subcellular localization and relevance to the neurotoxic property have not been well characterized. Hence, GFP version of PrP(1–144) transgene was constructed and transfected in two independent cell lines, N2a and HpL3-4 cells.

Here we demonstrate for the first time that GFP-PrP(1–144) exhibited an aberrant mitochondrial localization accompanied by the depolarization of mitochondrial innermembrane, cytochrome *c* release in the cytosol, DNA fragmentation, and the formation of numerous PrP-containing deposits in intracellular vacuoles resembling secondary lysosomes.

Materials and methods

Construction of GFP-PrP and GFP-PrP(1–144). GFP-PrP constructs were made as previously described [4,6], and the resulted plasmid was designated pSPOX-MHM2PrP::GFP. The mutant was amplified by PCR from the pSPOX-MHM2PrP::GFP (for amino acid residues Δ 144–230 in mouse PrP) [4,6], digested with *Bam*HI and *Xho*I, and replaced with the *Bam*HI–*Xho*I fragment of pSPOX-MHM2PrP::GFP [14]. Non-fluorescent PrP constructs were made from the pSPOX-MHM2PrP [14]. The resulted plasmid was verified by direct DNA sequencing.

Antibodies and drugs. Antibody K3 against PrP^C was rabbit polyclonal sera raised against N-terminal PrP peptides corresponding to

residues 76–90 in mouse PrP. Anti-cytochrome *c* and anti-porin were purchased from BD Biosciences. Anti-Hsc70 and anti-BiP were purchased from Stressgen Biotechnologies. Anti-GFP was purchased from Sigma. Mitotracker Red CMXRos was purchased from Molecular Probes. Lactacystin, ALLN, and MG132 were purchased from Sigma. The mitochondrial innermembrane potential ($\Delta\Psi_m$) detection kit was purchased from Trevigen. DNA fragmentation was measured by TUNEL (APO-BrdU TUNEL assay kit (Molecular Probes)), which was performed according to the manufacturer's instructions before being visualized with a Delta-Vision microscopy system (Applied Precision), and out-of-focus images were removed by interactive deconvolution. Antibodies were used at 1:1000 (Western blotting) or 1:100 (immunoelectron microscopy) unless otherwise noted. For immunoelectron microscopy, 10 and 20 nm golds were purchased from DAKO.

Cell cultures, DNA transfection, and drug treatments. Mouse N2a cells were obtained from American Tissue Culture Collection, and HpL3-4 cells were provided by Dr. T. Onodera (the University of Tokyo). Cells were grown and maintained at 37 °C in MEM supplemented with 10% fetal bovine serum. N2a and HpL3-4 cells were transiently transfected with each construct using a DNA transfection kit (Lipofectamin, Gibco-BRL). Western blot analyses were performed as described [14]. To inhibit proteasomal function, N2a or HpL3-4 cells were treated with 10 μ M lactacystin, ALLN, or MG132 for 3.5 h at 37 °C.

Preparation of mitochondrial, microsomal, and cytosolic fractions [15]. Cells were homogenized with 9 volumes of mitochondrial buffer (220 mM mannitol, 70 mM sucrose, 10 mM Hepes–KOH, pH 7.4, and 0.1 mM EDTA) and centrifuged at 700g for 5 min at 4 °C, and the supernatant was further centrifuged at 5000g for 10 min at 4 °C. The supernatant was used as a post-mitochondrial supernatant. The resulted pellet was washed three times with mitochondrial buffer, resuspended in 9 volumes of the same buffer, and then centrifuged at 2000g for 2 min at 4 °C followed by 5000g for 8 min at 4 °C. The pellet was resuspended in 9 volumes of the same buffer and then centrifuged at 5000g for 10 min at 4 °C. The final pellet was recovered and stored on ice until use (mitochondrial fraction). The post-mitochondrial supernatant was further centrifuged at 100,000g for 1 h at 4 °C, and the supernatant was used as cytosolic fraction, and the pellet was resuspended in mitochondrial buffer (microsomal fraction). Western blots were performed at 5 μ g total protein/lane.

Real-time imaging. To observe living cells, cells were cultured on glass-bottomed dishes (Matsunami) for 24–48 h after the DNA transfection. To visualize mitochondria, cells were incubated for 10 min at 37 °C with Mitotracker Red CMXRos at desired concentrations. Images of cells were collected with a Delta Vision Microscopy System (Applied Precision) equipped with an Olympus IX70.

Results

The intracellular localization of fluorescent PrP^C was investigated through the real-time imaging in living cells by utilizing GFP-PrP constructs. It was investigated in N2a cells that can be infected with PrP^{Sc} [16] and has been widely used for studies in the PrP^C metabolism, as well as in HpL3-4 cells, a hippocampal cell line established from *prnp* gene-ablated mice [5].

GFP-PrP(1–144) exhibited an aberrant localization to mitochondria, as demonstrated by its colocalization with the mitochondrial-specific molecule, Mitotracker, in N2a cells (Fig. 1A, upper panels) and HpL3-4 cells (Fig. 1A, lower panels), whereas full-length GFP-PrP did not. Previously, we also demonstrated that GFP-

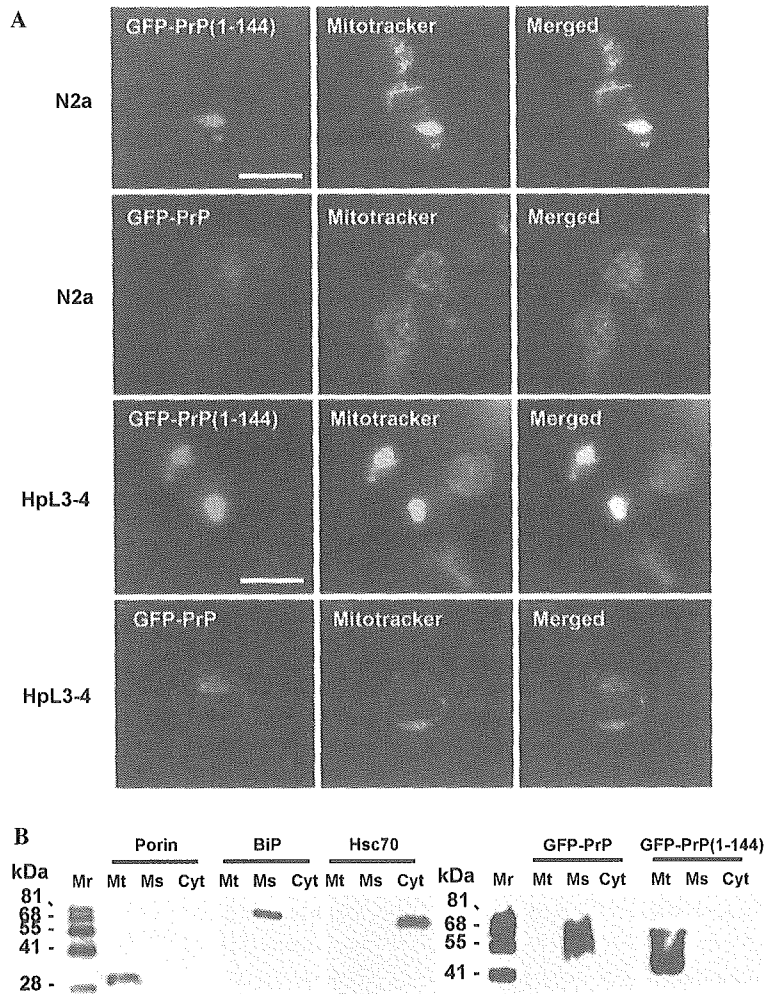


Fig. 1. Mitochondrial localization of GFP-PrP(1–144). GFP-PrP(1–144) exhibits aberrant localization in N2a cells, whereas full-length GFP-PrP does not. (A) GFP-PrP^C localization. Full-length GFP-PrP and GFP-PrP(1–144) constructs were made and transfected in N2a (upper panels) and HpL3-4 cells (lower panels). Scale bars = 8 μ m. (B) Western blot analysis with anti-GFP antibody. Anti-porin antibody was used as a mitochondrial (Mt) marker, anti-BiP antibody was used as a microsome (Ms) marker, and anti-Hsc70 antibody was used as a cytosolic (Cyt) marker. Mr, molecular weight marker.

PrP(1–121) does not exhibit such mitochondrial localization [4]. Thus, the mitochondrial localization of GFP-PrP(1–144) requires not only PrP residues 121–144 (in human sequence) but also COOH-terminal truncation in the current experimental condition, regardless of whether endogenous full-length PrP^C exists. The aberrant mitochondrial localization of GFP-PrP(1–144) was further confirmed by Western blot analysis using a subcellular fractionation method (Fig. 1B).

Subsequently, the GFP-PrP(1–144) induced the depolarization of mitochondrial innermembrane (a change in the $\Delta\Psi_m$) in N2a (Fig. 2A, upper panels) and HpL3-4 cells (Fig. 2A, lower panels), release of cytochrome *c* from the intermembrane space into the cytosol (Fig. 2B), and DNA fragmentation assessed by TUNEL in N2a (Fig. 2C, upper panels) and HpL3-4 cells (data not shown). The PrP(1–144) is normally degraded through the proteasomal pathway, but intracellular

accumulation results if proteasomal degradation is impaired [13]. Therefore, we next set out to treat the non-fluorescent PrP(1–144)-transfected cells with proteasome inhibitors including lactacystin, ALLN, or MG132. After the lactacystin treatment, non-fluorescent PrP(1–144) induced the DNA fragmentation in N2a (Fig. 2C, lower panels) and HpL3-4 cells (data not shown). Treatment with ALLN or MG132 also exhibited similar results (data not shown). These observations are characteristic of the mitochondria-mediated apoptotic process. In contrast, none of these abnormalities was observed in N2a and HpL3-4 cells transfected with full-length GFP-PrP construct.

During these investigations, we noticed that GFP-PrP(1–144)-transfected N2a and HpL3-4 cells lost its normal mitochondrial configurations as if congregated predominantly in an intracellular perinuclear region. To further investigate the ultrastructural

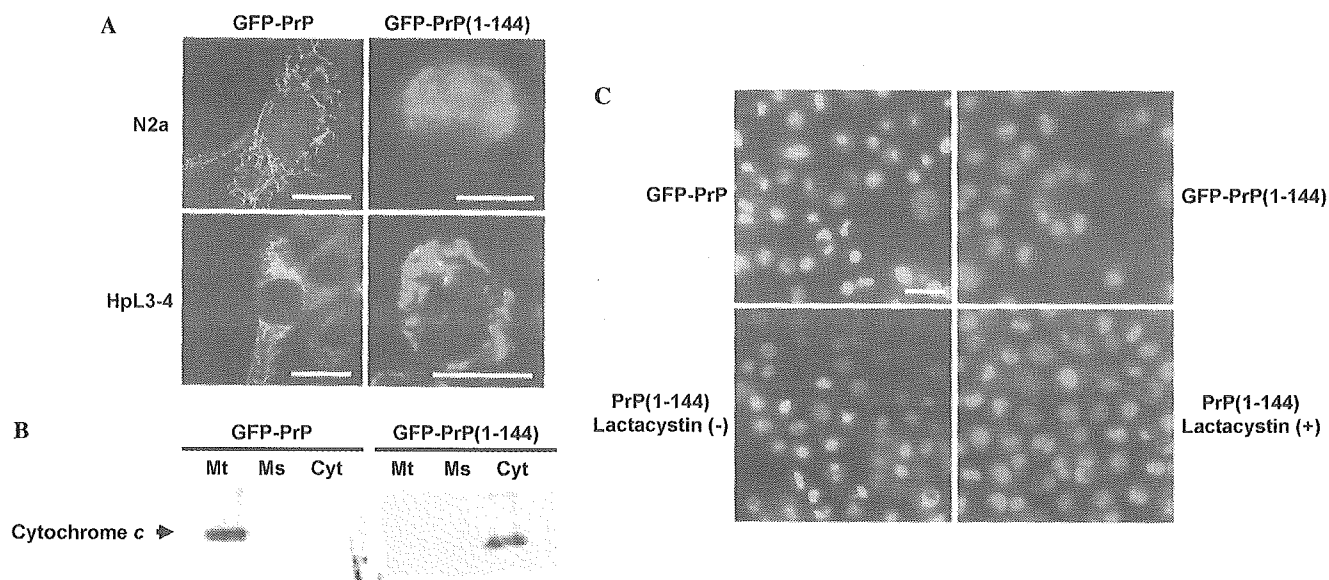


Fig. 2. Accumulation of GFP-PrP(1–144) induces mitochondria-mediated apoptosis. (A) Inactivation of the mitochondrial innermembrane potential ($\Delta\Psi_m$, red; active, green; inactive) in N2a (upper panels) and Hpl3-4 (lower panels) cells transfected with GFP-PrP(1–144). Scale bars = 4 μm . (B) The release of cytochrome *c* from the mitochondria in N2a cells transfected with GFP-PrP(1–144). Mt, mitochondria fraction; Ms, microsome fraction; and Cyt, cytosolic fraction. The markers are the same as shown in Fig. 1B. (C) Upper panels: DNA fragmentations measured by TUNEL (red; negative, green; positive) are shown in N2a cells transfected with GFP-PrP(1–144). Lower panels: non-fluorescent PrP(1–144) transfected in N2a cells also exhibits the DNA fragmentation in a lactacystin-dependent manner. Scale bars = 15 μm .

morphology of these mitochondria, we next performed electron microscopy in N2a cells transfected with GFP-PrP(1–144) in comparison with full-length GFP-PrP.

As results, numerous electron-dense deposits were observed in mitochondrial clusters of the GFP-PrP(1–144)-transfected N2a cells, whereas none was detected in N2a cells transfected with full-length GFP-PrP (Fig. 3A). Some vesicles contained myelin-like figures resembling those found in autophagic vacuoles forming secondary lysosomes (Fig. 3B). Co-localization of PrP-immunogolds (Fig. 3C, left panel)/GFP-immunogolds (Fig. 3C, middle panel) with porin-immunogold particles as a mitochondrial marker (Fig. 3C, right panel) was observed in such electron-dense vesicular foci. Non-fluorescent PrP(1–144) also induced the same deposits after the proteasomal inhibition (data not shown).

Discussion

The Y145STOP mutation at PrP residue 145 results in a heritable human prion disease, GSS-like disorder, with extensive PrP amyloid deposits in cerebral parenchyma and vessels [12,17]. The Y145STOP, which yields a product of PrP(1–144), lacks GPI-anchor and is normally degraded through the proteasomal pathway, and also results in intracellular accumulation if proteasomal degradation is impaired [13]. Most

PrP(1–144) is degraded very rapidly by the proteasome-mediated pathway, and thus blockage of proteasomal degradation results in intracellular accumulation of PrP(1–144). From the current results, however, the GFP-tagged PrP(1–144) seems to be more metabolically stable, and therefore GFP-PrP(1–144) expression itself is sufficient to induce its intracellular accumulation. In fact, non-fluorescent PrP(1–144) required the treatment with proteasome inhibitors to exhibit the same features.

In this paper, we revealed for the first time the site of intracellular accumulation and the neurotoxic property of mutant PrP^C, Y145STOP, in a human GSS model. The GFP-PrP(1–144) exhibited an aberrant localization to mitochondria, and subsequent mitochondria-mediated apoptosis was induced. Misfolded PrP^C is subjected to degradation by proteasomes, and accumulation of PrP^C in the cytosol is strongly neurotoxic in transgenic mice [18] and cyclosporin A-treated cultured cells [19], and proteasome inhibitors increase PrP^C-like immunoreactivity and unmasked a basal caspase 3 activation [20]. Concomitant with decreased proteasomal activity, aberrant mitochondrial localization of PrP^C followed by mitochondria-mediated neuronal apoptosis was also detected in aged transgenic mice overexpressing wild-type mouse PrP^C, but only after 520 days after birth [15]. These mice develop a spontaneous neurological dysfunction in an age-dependent manner [21,22]. Taken together, a PrP^C load in the cytosol induces the mitochondrial localization of PrP^C with subsequent mito-

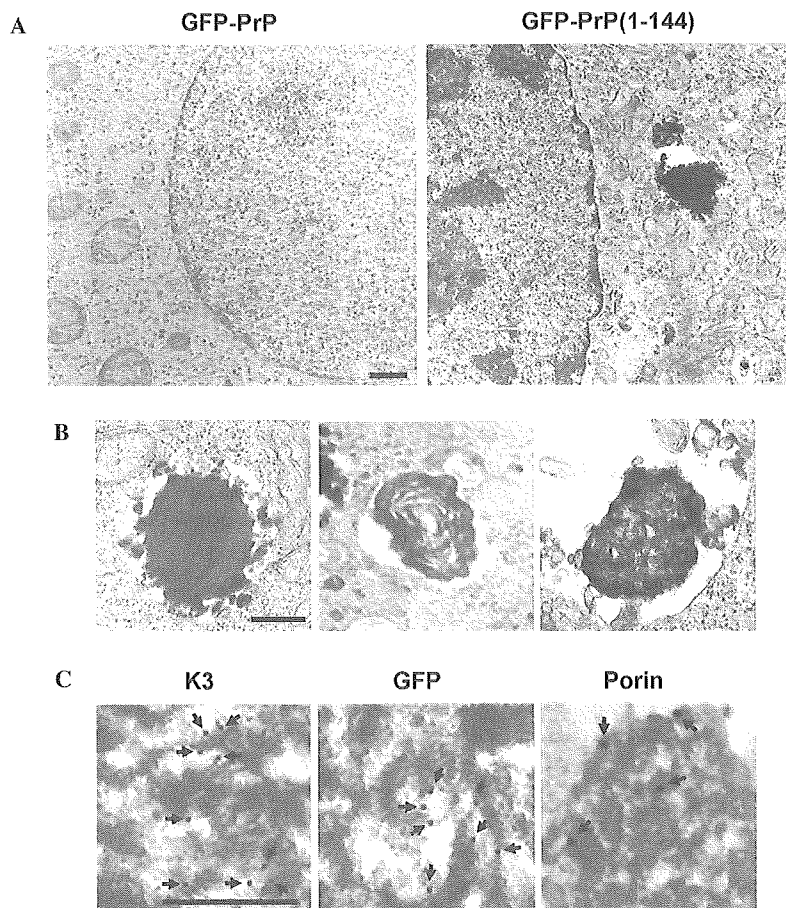


Fig. 3. GFP-PrP(1–144)-related electron-dense deposits. Scale bars = 0.1 μ m. (A) Electron microscopy (30,000 \times) detects numerous electron-dense deposits in N2a cells transfected with GFP-PrP(1–144), whereas full-length GFP-PrP induces no deposit. (B) Some vesicles contain myelin-like figures. (C) Immunoelectron microscopy (30,000 \times) detects GFP-PrP(1–144) with anti-PrP antibody K3 (10 nm golds, left panel) or anti-GFP antibody (10 nm golds, middle panel) within the electron dense deposits of N2a cells. Anti-porin antibody (20 nm golds) also stains the deposits (right panel).

chondria-mediated apoptosis. Consequently, such neurotoxic property may contribute to a common pathogenic mechanism shared in various PrP-related disorders.

Deposition of numerous electron-dense deposits immunostained with anti-PrP antibody is another characteristic in GFP-PrP(1–144)-transfected cells, and has not been reported in other studies so far. The relevance of such electron-dense deposits with PrP amyloid deposits, a characteristic feature of human GSS with Y145STOP, is an intriguing question. These amyloid plaques were composed of COOH-terminal truncated PrP [12], but have not transmitted to mice [17]. Of note, both the electron-dense deposits in Y145STOP-transfected N2a cells and PrP^{Sc} in scrapie-infected N2a cells were found in the similar vacuolar compartment resembling secondary lysosomes [23], suggesting that both deposits may share a similar resistance to such a harsh lysosomal condition.

The Y145STOP mutation has been widely investigated in terms of its biochemical property. Peptides

encompassing PrP(89–143) when mixed with PrP^C produced fibrous aggregates and displayed a high β -sheet content, although no prion infectivity was observed [24,25]. Recently, Kundu et al. [26] reported a spontaneous conversion of the recombinant polypeptide, human PrP(23–144), from a monomeric unordered state to a fibrillar form, in which human PrP residues within the 138–141 region are essential. Interestingly, this conversion has characteristics of a nucleation-dependent polymerization. Whether the numerous electron-dense deposits may serve as a seed for the growth of amyloid plaques with Y145STOP awaits further investigations.

Our current observations may provide clues as to the yet unknown underlying mechanism concerning the heritable human prion disease with Y145STOP at least in part. At the same time, the prion disease with Y145STOP has untransmitted to mice [17]. How this relates to the puzzle in prion biology, the discrepancy between the infectious and neurotoxic properties of PrP [27], remains to be further examined.

Acknowledgments

We greatly thank T. Onodera for providing the HpL3-4 cell line, E. Nannri, K. Ishibashi, C. Ota, and S. Wajima for technical assistances. This work was supported by grants from the Core Research for Evolutional Science and Technology (CREST) of Japan Science and Technology Corporation, Health and Labour Sciences Research Grants, Research on Advanced Medical Technology, nano-001, the Ministry of Agriculture, Forestry and Fisheries, and the Ministry of Health, Labor, and Welfare of Japan.

References

- [1] S.B. Prusiner, Prions, *Proc. Natl. Acad. Sci. USA* 95 (1998) 13363–13383.
- [2] S.B. Prusiner, Shattuck lecture—neurodegenerative diseases and prions, *N. Engl. J. Med.* 344 (2001) 1516–1526.
- [3] J. Collinge, Variant creutzfeldt-Jakob disease, *Lancet* 354 (1999) 317–323.
- [4] N.S. Hachiya, K. Watanabe, Y. Sakasegawa, K. Kaneko, Microtubules-associated intracellular localization of the NH(2)-terminal cellular prion protein fragment, *Biochem. Biophys. Res. Commun.* 313 (2004) 818–823.
- [5] C. Kuwahara, A.M. Takeuchi, T. Nishimura, K. Haraguchi, A. Kubosaki, Y. Matsumoto, K. Saeki, T. Yokoyama, S. Itohara, T. Onodera, Prions prevent neuronal cell-line death, *Nature* 400 (1999) 225–226.
- [6] N.S. Hachiya, K. Watanabe, M. Yamada, Y. Sakasegawa, K. Kaneko, Anterograde and retrograde intracellular trafficking of fluorescent cellular prion protein, *Biochem. Biophys. Res. Commun.* 315 (2004) 802–807.
- [7] K.S. Lee, A.C. Magalhaes, S.M. Zanata, R.R. Brentani, V.R. Martins, M.A. Prado, Internalization of mammalian fluorescent cellular prion protein and N-terminal deletion mutants in living cells, *J. Neurochem.* 79 (2001) 79–87.
- [8] A.C. Magalhaes, J.A. Silva, K.S. Lee, V.R. Martins, V.F. Prado, S.S.G. Ferguson, M.V. Gomez, R.R. Brentani, M.A.M. Prado, Endocytic intermediates involved with the intracellular trafficking of a fluorescent cellular prion protein, *J. Biol. Chem.* 277 (2002) 33311–33318.
- [9] A. Negro, C. Ballarin, A. Bertoli, M.L. Massimino, M.C. Sorgato, The metabolism and imaging in live cells of the bovine prion protein in its native form or carrying single amino acid substitutions, *Mol. Cell. Neurosci.* 17 (2001) 521–538.
- [10] H. Lorenz, O. Windl, H.A. Kretzschmar, Cellular phenotyping of secretory and nuclear prion proteins associated with inherited prion diseases, *J. Biol. Chem.* 277 (2002) 8508–8516.
- [11] L. Ivanova, S. Barmada, T. Kummer, D.A. Harris, Mutant prion proteins are partially retained in the endoplasmic reticulum, *J. Biol. Chem.* 276 (2001) 42409–42421.
- [12] T. Kitamoto, R. Iizuka, J. Tateishi, An amber mutation of prion protein in Gerstmann–Straussler syndrome with mutant PrP plaques, *Biochem. Biophys. Res. Commun.* 192 (1993) 525–531.
- [13] G. Zanusso, R.B. Petersen, T. Jin, Y. Jing, R. Kanoush, S. Ferrari, P. Gambetti, N. Singh, Proteasomal degradation and N-terminal protease resistance of the codon 145 mutant prion protein, *J. Biol. Chem.* 274 (1999) 23396–23404.
- [14] M.R. Scott, R. Kohler, D. Foster, S.B. Prusiner, Chimeric prion protein expression in cultured cells and transgenic mice, *Protein Sci.* 1 (1992) 986–997.
- [15] N.S. Hachiya, M. Yamada, K. Watanabe, A. Jozuka, T. Ohkubo, K. Sano, Y. Takeuchi, Y. Kozuka, Y. Sakasegawa, K. Kaneko, Mitochondrial localization of cellular prion protein (PrPc) invokes neuronal apoptosis in aged transgenic mice overexpressing PrPc, *Neurosci. Lett.*, in press.
- [16] D.A. Butler, M.A. Scott, J.M. Bockman, D.R. Borchelt, A. Taraboulos, K.K. Hsiao, D.T. Kingsbury, S.B. Prusiner, Scrapie-infected murine neuroblastoma cells produce protease-resistant prion proteins, *J. Virol.* 62 (1988) 1558–1564.
- [17] J. Tateishi, T. Kitamoto, Inherited prion diseases and transmission to rodents, *Brain Pathol.* 5 (1995) 53–59.
- [18] J. Ma, R. Wollmann, S. Lindquist, Neurotoxicity and neurodegeneration when PrP accumulates in the cytosol, *Science* 298 (2002) 1781–1785.
- [19] E. Cohen, A. Taraboulos, Scrapie-like prion protein accumulates in aggregates of cyclosporin A-treated cells, *EMBO J.* 22 (2003) 404–417.
- [20] E. Paitel, C. Alves da Costa, D. Vilette, J. Grassi, F. Checler, Overexpression of PrPc triggers caspase 3 activation: potentiation by proteasome inhibitors and blockade by anti-PrP antibodies, *J. Neurochem.* 83 (2002) 1208–1214.
- [21] D. Westaway, J. Cayetano-Canlas, D. Groth, D. Foster, S.-L. Yang, M. Torchia, G.A. Carlson, S.B. Prusiner, Degeneration of skeletal muscle, peripheral nerves, and the central nervous system in transgenic mice overexpressing wild-type prion proteins, *Cell* 76 (1994) 117–129.
- [22] V. Perrier, K. Kaneko, J. Safar, J. Vergara, P. Tremblay, S.J. DeArmond, F.E. Cohen, S.B. Prusiner, A.C. Wallace, Dominant-negative inhibition of prion replication in transgenic mice, *Proc. Natl. Acad. Sci. USA* 99 (2002) 13079–13084.
- [23] M.P. McKinley, A. Taraboulos, L. Kenaga, D. Serban, A. Stieber, S.J. DeArmond, S.B. Prusiner, N. Gonatas, Ultrastructural localization of scrapie prion proteins in cytoplasmic vesicles of infected cultured cells, *Lab. Invest.* 65 (1991) 622–630.
- [24] K. Kaneko, D. Peretz, K.M. Pan, T.C. Blochberger, H. Wille, R. Gabizon, O.H. Griffith, F.E. Cohen, M.A. Baldwin, S.B. Prusiner, Prion protein (PrP) synthetic peptides induce cellular PrP to acquire properties of the scrapie isoform, *Proc. Natl. Acad. Sci. USA* 92 (1995) 11160–11164.
- [25] K. Kaneko, H. Wille, I. Mehlhorn, H. Zhang, H. Ball, F.E. Cohen, M.A. Baldwin, S.B. Prusiner, Molecular properties of complexes formed between the prion protein and synthetic peptides, *J. Mol. Biol.* 270 (1997) 574–586.
- [26] B. Kundu, N.R. Maiti, E.M. Jones, K.A. Surewicz, D.L. Vanik, W.K. Surewicz, Nucleation-dependent conformational conversion of the Y145Stop variant of human prion protein: structural clues for prion propagation, *Proc. Natl. Acad. Sci. USA* 100 (2003) 12069–12074.
- [27] R. Chiesa, P. Piccardo, E. Quaglio, B. Drisaldi, S.L. Si-Hoe, M. Takao, B. Ghetti, D.A. Harris, Molecular distinction between pathogenic and infectious properties of the prion protein, *J. Virol.* 77 (2003) 7611–7622.



Mitochondrial localization of cellular prion protein (PrP^C) invokes neuronal apoptosis in aged transgenic mice overexpressing PrP^C

Naomi S. Hachiya^{a,b}, Makiko Yamada^{a,b}, Kota Watanabe^{a,b}, Akiko Jozuka^{a,b},
Takuya Ohkubo^{a,c}, Kenichi Sano^{a,1}, Yoshio Takeuchi^{a,2},
Yoshimichi Kozuka^d, Yuji Sakasegawa^a, Kiyotoshi Kaneko^{a,b,*}

^a *Departments of a Cortical Function Disorders, National Institute of Neuroscience (NIN), National Center of Neurology and Psychiatry (NCNP), Kodaira, Tokyo 187-8502, Japan*

^b *Core Research for Evolutional Science and Technology (CREST), Japan Science and Technology Agency, Kawaguchi, Saitama 332-0012, Japan*

^c *Department of Neurology and Neurological Science, Graduate School of Medicine, Tokyo Medical and Dental University, Bunkyo-ku, Tokyo 113-0034, Japan*

^d *Ultrastructural Research, National Institute of Neuroscience (NIN), National Center of Neurology and Psychiatry (NCNP), Kodaira, Tokyo 187-8502, Japan*

Received 14 September 2004; received in revised form 12 October 2004; accepted 13 October 2004

Abstract

Recent studies suggest that the disease isoform of prion protein (PrP^{Sc}) is non-neurotoxic in the absence of cellular isoform of prion protein (PrP^C), indicating that PrP^C may participate directly in the neurodegenerative damage by itself. Meanwhile, transgenic mice harboring a high-copy-number of wild-type mouse (Mo) PrP^C develop a spontaneous neurological dysfunction in an age-dependent manner, even without inoculation of PrP^{Sc} and thus, investigations of these aged transgenic mice may lead to the understanding how PrP^C participate in the neurotoxic property of PrP. Here we demonstrate mitochondria-mediated neuronal apoptosis in aged transgenic mice overexpressing wild-type MoPrP^C (Tg(MoPrP)4053/FVB). The aged mice exhibited an aberrant mitochondrial localization of PrP^C concomitant with decreased proteasomal activity, while younger littermates did not. Such aberrant mitochondrial localization was accompanied by decreased mitochondrial manganese superoxide dismutase (Mn-SOD) activity, cytochrome *c* release into the cytosol, caspase-3 activation, and DNA fragmentation, most predominantly in hippocampal neuronal cells. Following cell culture studies confirmed that decrease in the proteasomal activity is fundamental for the PrP^C-related, mitochondria-mediated apoptosis. Hence, the neurotoxic property of PrP^C could be explained by the mitochondria-mediated neuronal apoptosis, at least in part.

© 2004 Elsevier Ireland Ltd. All rights reserved.

Keywords: PrP^C; Proteasomal activity; Mitochondrial localization; Superoxide dismutase activity; Mitochondria-mediated apoptosis

The posttranslational conformational change of the cellular isoform of prion protein (PrP^C) into its scrapie isoform (PrP^{Sc}) is the fundamental process underlying the pathogenesis of prion diseases [24], but the molecular events through

which prion infection and the resulting accumulation of PrP lead to the neuronal dysfunction, vacuolation, and death that characterize prion pathology remain unclear [6].

Importantly, PrP^{Sc}, the disease isoform of PrP, seems to be non-neurotoxic in the absence of PrP^C, suggesting that PrP^C may participate directly in the prion neurodegenerative damage by itself, and the cellular pathways activated by neurotoxic forms of PrP that ultimately result in neuronal death are also being investigated, and several possible mechanisms have been uncovered [6]. For example, cross-linking

* Corresponding author. Tel.: +81 42 346 1718; fax: +81 42 346 1748.
E-mail address: kaneko@ncnp.go.jp (K. Kaneko).

¹ Present address: Hinoieda Kagaku Ltd., Hino-city, Tokyo 191-0061, Japan.

² Present address: KOHJIN-BIO Ltd., Sakado-city, Saitama 350-0214, Japan.

PrP^C in vivo with specific monoclonal antibodies was found to trigger neuronal apoptosis, suggesting that PrP^C functions in the control of neuronal survival [26]. In fact, neural tissues overexpressing PrP^C grafted into the brains of PrP^C-deficient mice develop the severe histopathological changes characteristic of prion disease when infected with prions, but no pathological changes were seen in PrP^C-deficient tissue, not even in the immediate vicinity of the grafts despite the presence of high levels of PrP^{Sc} [2]. In addition, interruption of PrP^C expression during an ongoing prion infection prevents neuronal loss and reverses early spongiform change [16]. The continued accumulation of PrP^{Sc} in this model after neuronal PrP^C depletion is likely to reflect prion replication predominantly in both microglia and astrocytes glial cells without PrP^C depletion, which support PrP^{Sc} replication. The PrP^{Sc} deposits colocalize with astrocytes in the brains of infected mice with neuronal PrP^C depletion, which was not seen in scrapie-infected control animals without PrP depletion. The fact that these mice remain asymptomatic indicates that even extensive extraneuronal PrP^{Sc} replication does not cause clinical disease or neurodegeneration in this model. Thus, neuronal PrP^C seems to be fundamental for the neurotoxic property of PrP even in the PrP^{Sc}-infected conditions, but the detailed molecular events especially with non-mutant, wild-type PrP^C still remained unclear.

Meanwhile, aged transgenic mice harboring a high-copy-number of wild-type PrP-B transgenes spontaneously developed mitochondrial encephalomyopathy including focal vacuolation of the central nervous system, skeletal muscles and peripheral nerves without PrP^{Sc} inoculation [28]. Such focal vacuolation was localized to the hippocampus, the superior colliculus, and midbrain tegmentum, which resembled that seen in experimental scrapie, albeit less intense. Other transgenic lines harboring a high-copy-number of wild-type PrP transgenes also exhibited spontaneous neurological dysfunction in an age-dependent manner [21,27]. For example, transgenic mice overexpressing the wild-type mouse (Mo) PrP-A gene (Tg(MoPrP)4053/FVB) used in this study became symptomatic at around the age of 700 days, although no pathological evidence for prion diseases was evident [27]. Since no PrP^{Sc} has been inoculated in these mice, investigations of these aged transgenic mice overexpressing wild-type PrP^C may lead to the better understanding how PrP^C participate in the neurotoxic property of PrP.

Here we show that the Tg(MoPrP)4053/FVB mice exhibited an aberrant mitochondrial localization of PrP^C accompanied by decreased mitochondrial manganese superoxide dismutase (Mn-SOD) activity, cytochrome *c* release in the cytosol, caspase-3 activation, and DNA fragmentation, concomitant with decreased proteasomal activity in an age-dependent manner.

Tg(MoPrP)4053/FVB and its littermate were kindly provided by Dr. S.B. Prusiner (University of California, San Francisco). Antibodies K3 and K4 against PrP were rabbit polyclonal sera raised against PrP peptides corresponding to residues 76–90 and 96–110 in MoPrP, respectively.

Anti-cytochrome *c* and anti-porin antibodies were purchased from BD Biosciences. Anti-Hsc70 antibody was purchased from Stressgen Biotechnologies Corporation. Mitotracker Red CMXRos was purchased from Molecular Probes. Lactacystin, ALLN, and MG132 were purchased from Sigma. The $\Delta\Psi_m$ detection kit and APO-BrdU TUNEL assay kit were purchased from Trevigen Inc. and Molecular Probes, respectively. Antibodies were used at 1:1000 (Western blotting) or 1:100 (immunofluorescence microscopy) unless otherwise noted. For immuno-electronmicroscopy, 10 nm golds were purchased from DAKO.

Cells or brains were homogenized with 9 volumes of mitochondrial buffer (220 mM mannitol, 70 mM sucrose, 10 mM Hepes-KOH, pH 7.4, and 0.1 mM EDTA) and centrifuged at $700 \times g$ for 5 min at 4 °C, and the supernatant was further centrifuged at $5000 \times g$ for 10 min at 4 °C. The supernatant was used as a post-mitochondrial supernatant. The resulted pellet was washed three times with mitochondrial buffer, re-suspended in 9 volumes of the same buffer, and then centrifuged at $2000 \times g$ for 2 min at 4 °C followed by $5000 \times g$ for 8 min at 4 °C. The pellet was resuspended in 9 volumes of the same buffer, and then centrifuged at $5000 \times g$ for 10 min at 4 °C. The final pellet was recovered and stored on ice until use (mitochondrial fraction). The post-mitochondrial supernatant was further centrifuged at $100,000 \times g$ for 1 h at 4 °C, and the supernatant was used as cytosolic fraction, and the pellet was resuspended in mitochondrial buffer (microsome fraction). Western blots were performed at 5 μ g of total protein/lane.

Mitochondrial manganese superoxide dismutase (Mn-SOD) and cytosolic copper/zinc SOD (Cu/Zinc-SOD) activities were measured by the SOD assay kit (Dojindo Molecular Technologies, Inc.), and cytosolic glutathione (GSH) was measured by the Glutathione quantification kit (Dojindo Molecular Technologies, Inc.) according to the manufacturer's instructions. Caspase-3 activity was measured using the PARP Western Blot Kit (WAKO) according to the manufacturer's instructions. DNA fragmentation was measured by the TUNEL assay (ApopTag[®] Peroxidase *In situ* Apoptosis Detection Kit, CHEMICON International), which was performed according to the manufacturer's instructions before being visualized with an Olympus CX40 (Olympus Optical Co., Ltd.). Sections were counter-stained by 0.5% methyl green (WAKO) in 0.1 M sodium acetate (pH 4.0).

Proteasomal activity assay was performed as previously described [3,9,31].

Tg(MoPrP)4053/FVB harboring a high-copy-number of wild-type PrP-A transgenes at the age of 520 days (TG520) and an age-matched non-transgenic littermate (WT520) showed similar migration rates of PrP^C on poly acrylamide gel electrophoresis and Western blotting using anti-PrP-antibody K4 (Fig. 1A, PK(–)). As increased resistance to protease K digestion is often a feature of PrP^{Sc}, this was examined in TG520 and WT520. No resistance to proteinase K digestion was detected in any of these mice (Fig. 1A, PK(+)). Histological examinations of the TG520 brains including

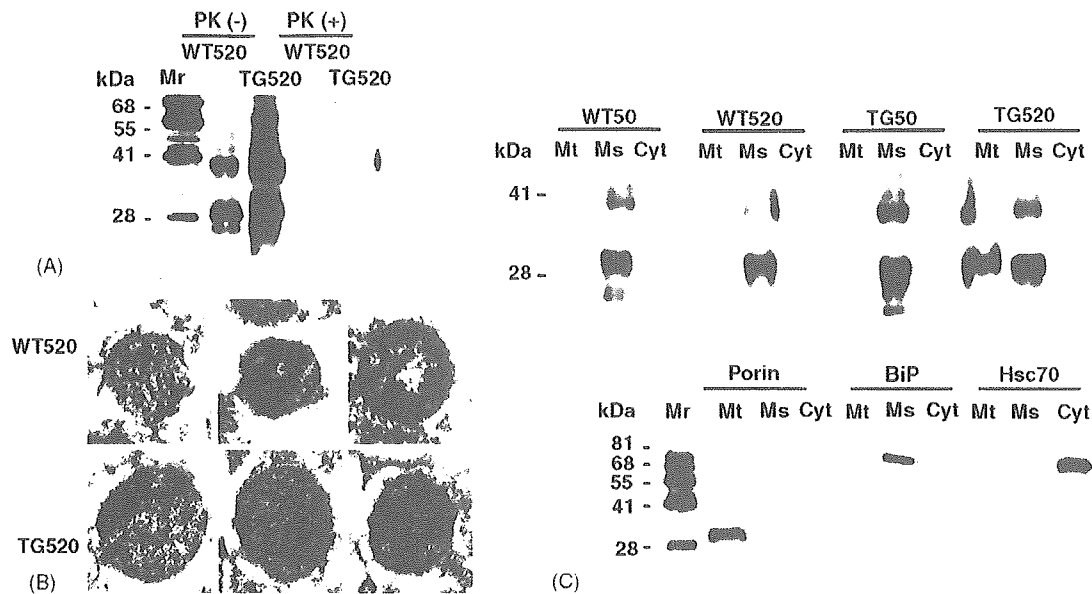


Fig. 1. PrP^C is localized to the mitochondrial fraction in Tg(MoPrP)4053/FVB overexpressing wild-type PrP^C. WT520: non-transgenic littermate at the age of 520 days. TG520: Tg(MoPrP)4053/FVB at the age of 520 days. WT50: non-transgenic littermate at the age of 50 days. TG50: Tg(MoPrP)4053/FVB at the age of 50 days. (A) Western blot analysis and resistance to proteinase K digestion of PrP^C in WT520 and TG520. PK(-): Western blot analysis with anti-PrP antibody K4. Bands derived from PrP^C appear to be normal. PK(+): resistance to proteinase K digestion. Five hundred microliter of brain homogenates (5 μ g of total protein/lane) were digested with proteinase K (20 μ g/ml, Sigma) at 37 $^{\circ}$ C for 1 h followed by centrifugation at 100,000 \times g for 1 h at 4 $^{\circ}$ C and the resuspended pellet was loaded onto the gels. No resistance to proteinase K digestion is detected. Mr: molecular weight marker. (B) Immunoelectron microscopy (30,000 \times) detects PrP^C with anti-PrP K3 (10 nm golds) in the mitochondria of neuronal cells in TG520. (C) Total brain homogenates of TG520 exhibit aberrant localization of overexpressed PrP^C, whereas those of WT50, WT520 and TG50 do not. Western blot analysis with anti-PrP antibody K4 (1:1000). Anti-porin antibody (1:1000) was used as a mitochondrial (Mt) marker, anti-BiP antibody (1:1000) was used as a microsomal (Ms) marker, and anti-Hsc70 antibody (1:1000) was used as a cytosolic (Cyt) marker.

dentate gyrus, hippocampus, other cerebral cortices, basal ganglia and cerebellum by hematoxylin and eosin as well as methyl green-pyronin staining revealed no apparent pathological evidence in the brain sections of WT520 and TG520 (data not shown).

Since older transgenic mice (not inoculated with PrP^{Sc}) that harbor a high-copy-number of wild-type PrP-B transgenes develop mitochondrial encephalomyopathy including focal vacuolation of the central nervous system, skeletal muscles and peripheral nerves [28], we set out to determine whether PrP^C could be detected in the mitochondrial fraction of TG520. Although the TG520 appeared clinically and histologically normal, they exhibited aberrant mitochondrial localization of PrP^C as determined by immunoelectron microscopy; immunogold-labelled PrP^C localized at the mitochondria of the granular cells in the hippocampal dentate gyrus of TG520 but not of WT520 (Fig. 1B). Such aberrant mitochondrial localization of PrP^C was further confirmed in TG520 by Western blotting using a subcellular fractionation, whereas younger non-transgenic littermate at the age of 50 days (WT50), WT520, and younger Tg(MoPrP)4053/FVB at the age of 50 days (TG50) did not exhibit the feature (Fig. 1C).

The oxidative stress leads to dysfunctions of the respiratory enzymes and the depletion of ATP followed by a decrease in reduced glutathione (GSH) concentration, which triggers the cycle of oxidative stress, mitochondrial dysfunction,

and further antioxidant depletion. Exposure of tissue to oxygen free radicals results in lipid peroxidation, protein oxidation and DNA damage, which is in concert with "apoptosis". In order to prevent such damages, mammalian cells are equipped with both non-enzymatic and enzymatic scavenging systems to eliminate oxygen free radicals, anti oxidant enzymes, i.e., SOD, catalase, and glutathione peroxidase are essential to cells in removing O₂⁻ and hydrogen peroxide (H₂O₂) from the tissues exposed to oxidative stress. Therefore, we next examined mitochondrial Mn-SOD as well as cytosolic Cu/Zn-SOD activities.

The mitochondrial Mn-SOD activity decreased significantly in TG520 compared to that in WT50, TG50, or WT520 (Fig. 2A), whereas no significant difference in the cytosolic copper/zinc SOD (Cu/Zn-SOD) activity was observed among them (Fig. 2B). Furthermore, cytosolic GSH level was dramatically decreased in TG520 but not in WT50, TG50, or WT520 (Fig. 2C). These results indicated that mitochondrial-localized PrP^C induced oxidative stress in TG520.

Subsequently, release of cytochrome *c* from the inner-membrane space into the cytosol (Fig. 3A), caspase-3 activation (Fig. 3B), and DNA fragmentation (Fig. 3C) were observed in TG520 brain, whereas no release of cytochrome *c*/DNA fragmentation but faint caspase-3 activation was detected in WT520 brain (Fig. 3A–C). Serial specimens of TG520 and WT520 brains were further examined by

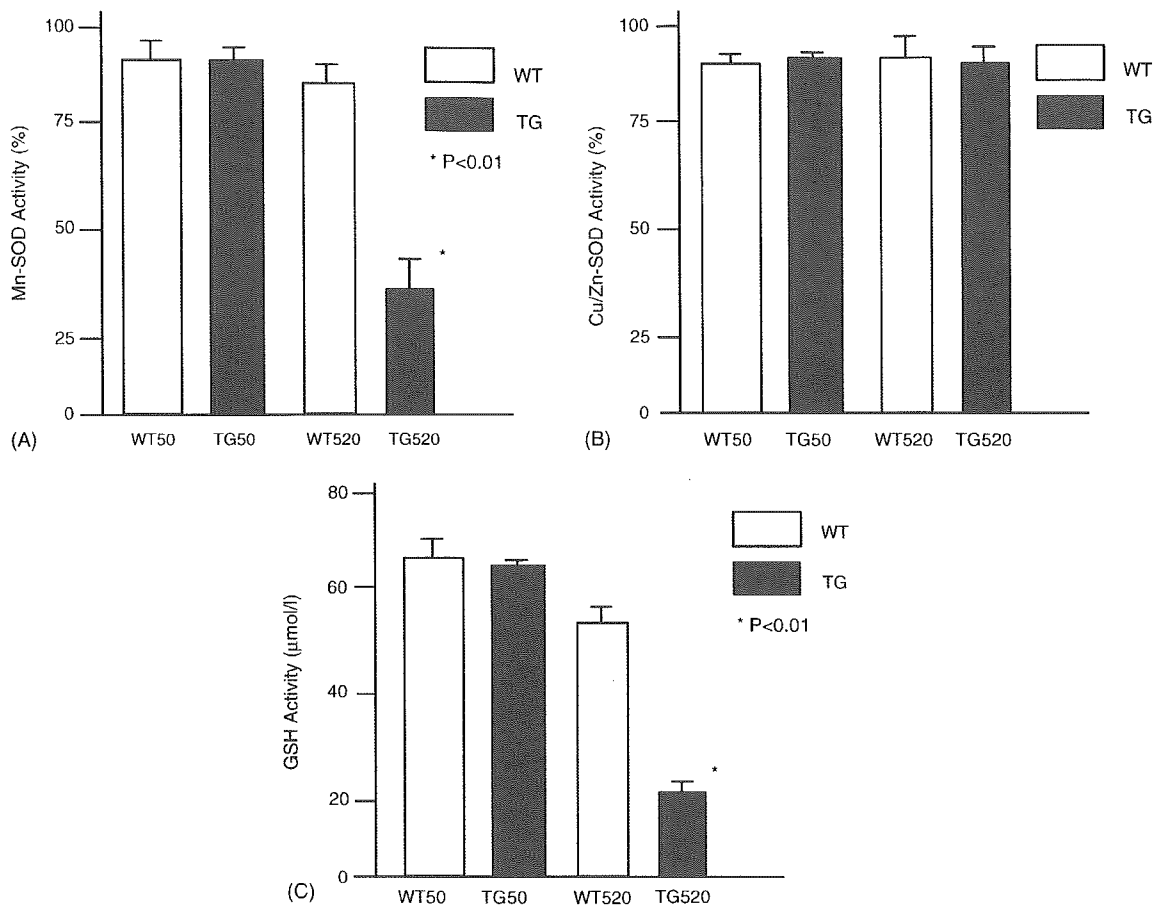


Fig. 2. Mitochondria-localized PrP^C induces oxidative stress in TG520. (A) Mitochondrial manganese superoxide dismutase (Mn-SOD) and (B) cytosolic copper/zinc SOD (Cu/Zinc-SOD) activities. The Mn-SOD activity decreases significantly in TG520 compared to that in WT50, TG50 or WT520, whereas the cytosolic Cu/Zn-SOD activity remained similar among them. Error bars represent mean \pm S.D. (C) Cytosolic glutathione (GSH) level is dramatically decreased in TG520 but not in WT50, TG50, or WT520. Error bars represent mean \pm S.D.

the TUNEL assay (Fig. 3D). As shown, the TUNEL assay showed that the DNA fragmentation most predominantly in granular cells in the hippocampal dentate gyrus and to a lesser extent pyramidal cells in the CA1 and CA2 regions of TG520 (Fig. 3D).

In an age-dependent development of other aggregation disorders, the accumulation and aggregation of the disease related-proteins are associated with an age-dependent decrease in proteasomal activity and are promoted by inhibition of proteasomal activity [31]. Therefore, it is also likely that such aberrant mitochondrial localization requires PrP^C retained in the cytoplasm with the proteasomal activity decreased. Therefore, the hydrolysis of Suc-Leu-Leu-Val-Tyr-4-methyl-coumaryl-7-amide (Suc-LLVY-MCA) by chymotrypsin-like proteasomal activity in brain homogenates of WT50, WT520, TG50, and TG520 was then investigated. As expected, proteasomal activity of both transgenic mice Tg(MoPrP)4053/FVB and non-transgenic littermate decreased with increasing age (Fig. 3E).

The posttranslational conformational change of PrP^C into PrP^{Sc} is the fundamental process underlying the pathogene-

sis of prion diseases [24]. Many concurrent reports have suggested that PrP^C may play a role in neuronal survival or death. The removal of serum from cells in culture causes apoptosis in PrP^C-deleted cells but not in wild-type cells [13]. PrP^C also inhibits Bax-mediated neuronal apoptosis in human primary neurons [1]. The binding of a ligand to PrP^C transduces neuroprotective signaling through a cAMP/PKA-dependent pathway. Therefore, PrP^C may function as a trophic receptor whose activation results in a neuroprotective state [5].

On the other hand, misfolded PrP^C is subject to degradation by proteasomes. Like many misfolded secretory proteins [12,23], it is recognized in the ER and subject to retrograde transport to the cytoplasm and degradation by the proteasome [11,14,29,30]. Or, a small fraction of PrP chains is not translocated into the ER lumen during synthesis, and is rapidly degraded in the cytoplasm by the proteasome as far as proteasome function remains normal [8]. As proteasome function gradually decreases with age over a very long period or with inhibitors in the case of cultured cells, PrP^C overflows in the cytoplasm, targeted to the mitochondria, which subsequently induces the mitochondria-mediated apoptosis.

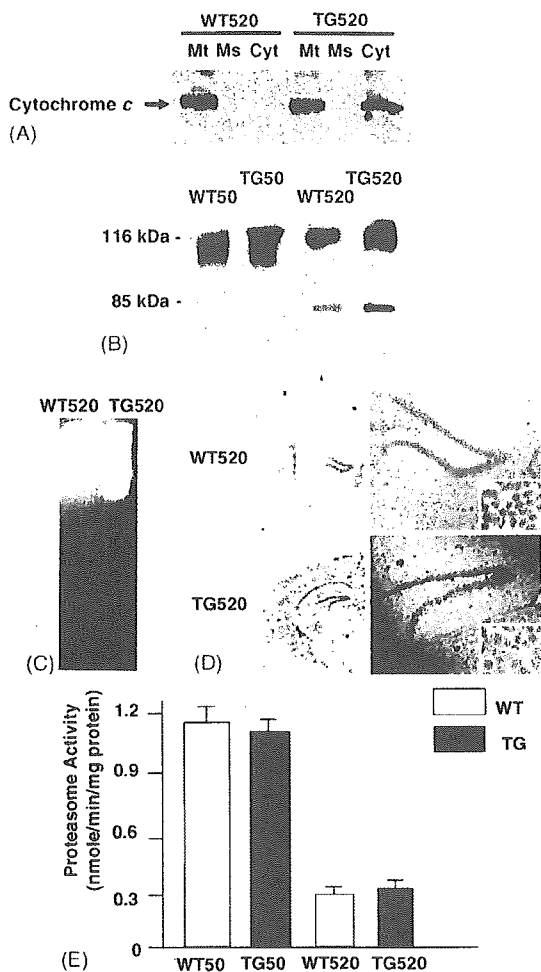


Fig. 3. Neuronal apoptosis in the TG520 brain. (A) Measurement of cytochrome *c* released into the cytosol. Western blot analysis with anti-cytochrome *c* antibody detects cytochrome *c* in the cytosol of the TG520 but not WT520 brain. Mt: mitochondrial fraction, Ms: microsomal fraction, Cyt: cytosolic fraction. (B) Caspase-3 activation in TG520 brain. Brain homogenates (5 μ g of total protein/lane) of younger WT50 and TG50 do not exhibit caspase-3 activation. Note that a faint band is detected in WT520 brain. The 85 kDa bands corresponding to the degradation products of poly ADP-ribose polymerase (PARP, 116 kDa) is a measure of caspase-3 activity. (C) DNA fragmentation in brain homogenates of TG520 is shown (1 μ g of genomic DNA/lane). Brain homogenates of WT520 show no DNA fragmentation. Genomic DNAs were applied onto 1% agarose gel. (D) Serial frozen sections of total brains (left panels) and the hippocampal regions (right panels, 40 \times , lower right corner panels, 400 \times) were made. Top panels: WT520. Bottom panels: TG520. Neuronal apoptosis (brown) is evident in the bottom panels as compared with the top panels. (E) Age-dependent decrease in brain proteasomal activity. Chymotrypsin-like proteolytic activity was assayed in brain homogenates (1 μ g of total protein/assay) of WT50, TG50, WT520, and TG520. Error bars represent mean \pm S.D. ($n = 3$).

In fact, accumulation of PrP^C in the cytoplasm is known to be strongly neurotoxic in both transgenic mice overexpressing the cytosolic form of PrP^C [15] and cyclosporin A-treated cultured cells [7]. In these systems, PrP^C expression enhances staurosporine-stimulated neuronal toxicity and DNA fragmentation, caspase-3-like activity and p53 transcriptional activities, all of which suggests that PrP^C sensitizes neurons

to apoptotic stimuli through caspase-3-mediated activation [20]. Proteasome inhibitors increase PrP^C-like immunoreactivity and unmask basal caspase-3 activation [19].

Despite these efforts, little is known about the PrP^C localization and its metabolic fate in the cytoplasm. Ma et al. reported that PrP accumulated in the cytoplasm when proteasomal activity was compromised, and PrP^C formed aggregates, often in association with Hsc70 [14]. With prolonged incubation, these aggregates accumulate in an "aggresome"-like state, surrounding the centrosome. Contrary to this report, other investigators reported there was a prominent shift in the intracellular locations of PrP immunostaining, but there was no "aggresome"-like PrP accumulation in the centrosome region [29]. The PrP signal was especially pronounced around the nucleus, and this signal only partially overlapped with both ER (calnexin, BiP and concanavalin A) and Golgi (wheat germ agglutinin). Thus, further examination has been awaited for determining the precise intracellular localization of PrP^C in the cytoplasmic face.

With an artificial PrP peptide corresponding to PrP residues 106–126 [PrP(106–126)], chronic exposure of primary rat hippocampal cultures to micromolar concentrations of the peptide induces neuronal death with DNA fragmentation in degenerating neurons, having indicated apoptotic cell death [10]. The earliest detectable apoptotic event was the rapid depolarization of mitochondrial membranes, occurring immediately following treatment of cells with PrP(106–126). Subsequently, cytochrome *c* was released and caspase-3 was activated. It has also been demonstrated that the fusogenic peptide PrP(118–135) induced time- and dose-dependent apoptosis in rat cortical and retinal neurons that included caspase-3 activation and DNA condensation/fragmentation [4,22]. These results have implicated mitochondria as the primary site of action [18]. Unfortunately, this implication has been restricted to the cell death with the artificial PrP peptides, and thereby further illustrates the significance of our current observations in terms of the neurotoxic property of wild-type PrP^C in vitro and in vivo.

There are potentially other mechanisms involved in neurotoxicity of the PrP^{Sc}-infected conditions, for example astrocytes, microglial cells and cytokines [17,25]. The activation of glial cells, which precedes neuronal death, and subsequent release of cytokines/chemokines may also contribute directly or indirectly to the neuronal cell death in prion diseases. In mutant PrP^C metabolism, on the other hand, the ER also seems to play another important role as well. Mutant PrP(Q217R) remains associated with the chaperone BiP at the ER for an abnormally long period of time and is degraded by the proteasomal pathway [11]. Nonetheless, our current observations suggest that wild-type PrP^C participate in the prion neurodegenerative cascade through the mitochondria-mediated events, at least in part. At the same time, the segregation of the infectious and neurotoxic properties of PrP suggests a new therapeutic strategy since prevention of mitochondrial mislocalization of PrP^C can be regarded as putative therapeutic targets aimed at protecting

cells from mitochondria-mediated apoptosis, even though the prion infection is not fully preventable.

Acknowledgements

We thank S.B. Prusiner for providing Tg(MoPrP)4053/FVB, T. Onodera for providing HpL3-4 cells, E. Nannri, K. Ishibashi, C. Ota, Y. Yamaura, and S. Wajima for technical assistance. We are indebted to G. Schatz, T. Omura, K. Mihara, R. Scheckman, and T. Momoi for helpful comments. This work was supported by grants from the Core Research for Evolutional Science and Technology (CREST) of the Japan Science and Technology Agency, Health and Labour Sciences Research Grants, Research on Advanced Medical Technology, nano-001, and the Ministry of Health, Labor and Welfare of Japan.

References

- [1] Y. Bounhar, Y. Zhang, C.G. Goodyer, A. LeBlanc, Prion protein protects human neurons against Bax-mediated apoptosis, *J. Biol. Chem.* 276 (2001) 39145–39149.
- [2] S. Brandner, S. Isenmann, A. Raeber, M. Fischer, A. Sailer, Y. Kobayashi, S. Marino, C. Weissmann, A. Aguzzi, Normal host prion protein necessary for scrapie-induced neurotoxicity, *Nature* 379 (1996) 339–343.
- [3] N. Canu, C. Barbato, M.T. Ciotti, A. Serafino, L. Dus, P. Calissano, Proteasome involvement and accumulation of ubiquitinated proteins in cerebellar granule neurons undergoing apoptosis, *J. Neurosci.* 20 (2000) 589–599.
- [4] J. Chabry, C. Ratsimanohatra, I. Spohne, P.P. Elena, J.P. Vincent, T. Pillot, In vivo and in vitro neurotoxicity of the human prion protein (PrP) fragment P118–135 independently of PrP expression, *J. Neurosci.* 23 (2003) 462–469.
- [5] L.B. Chiarini, A.R. Freitas, S.M. Zanata, R.R. Brentani, V.R. Martins, R. Linden, Cellular prion protein transduces neuroprotective signals, *EMBO J.* 21 (2002) 3317–3326.
- [6] R. Chiesa, D.A. Harris, Prion diseases: what is the neurotoxic molecule? *Neurobiol. Dis.* 8 (2001) 743–763.
- [7] E. Cohen, A. Taraboulos, Scrapie-like prion protein accumulates in aggregates of cyclosporin A-treated cells, *EMBO J.* 22 (2003) 404–417.
- [8] B. Drisaldi, R.S. Stewart, C. Adles, L.R. Stewart, E. Quaglio, E. Biasini, L. Fioriti, R. Chiesa, D.A. Harris, Mutant PrP is delayed in its exit from the endoplasmic reticulum, but neither wild-type nor mutant PrP undergoes retrotranslocation prior to proteasomal degradation, *J. Biol. Chem.* 278 (2003) 21732–21743.
- [9] M.E. Figueiredo-Pereira, K.A. Berg, S. Wilk, A new inhibitor of the chymotrypsin-like activity of the multicatalytic proteinase complex (20S proteasome) induces accumulation of ubiquitin-protein conjugates in a neuronal cell, *J. Neurochem.* 63 (1994) 1578–1581.
- [10] G. Forloni, N. Angeretti, R. Chiesa, E. Monzani, M. Salmona, O. Bugiani, F. Tagliavini, Neurotoxicity of a prion protein fragment, *Nature* 362 (1993) 543–546.
- [11] T. Jin, Y. Gu, G. Zanusso, M. Sy, A. Kumar, M. Cohen, P. Gambetti, N. Singh, The chaperone protein BiP binds to a mutant prion protein and mediates its degradation by the proteasome, *J. Biol. Chem.* 275 (2000) 38699–38704.
- [12] R.R. Kopito, ER quality control: the cytoplasmic connection, *Cell* 88 (1997) 427–430.
- [13] C. Kuwahara, A.M. Takeuchi, T. Nishimura, K. Haraguchi, A. Kubosaki, Y. Matsumoto, K. Saeki, T. Yokoyama, S. Itoharu, T. Onodera, Prions prevent neuronal cell-line death, *Nature* 400 (1999) 225–226.
- [14] J. Ma, S. Lindquist, Wild-type and PrP and a mutant associated with prion disease are subject to retrograde transport and proteasome degradation, *Proc. Natl. Acad. Sci. U.S.A.* 98 (2001) 14955–14960.
- [15] J. Ma, R. Wollmann, S. Lindquist, Neurotoxicity and neurodegeneration when PrP accumulates in the cytosol, *Science* 298 (2002) 1781–1785.
- [16] G. Mallucci, A. Dickinson, J. Linehan, P.C. Klohn, S. Brandner, J. Collinge, Depleting neuronal PrP in prion infection prevents disease and reverses spongiosis, *Science* 302 (2003) 871–874.
- [17] M. Marella, J. Chabry, Neurons and astrocytes respond to prion infection by inducing microglia recruitment, *J. Neurosci.* 24 (2004) 620–627.
- [18] C.N. O'Donovan, D. Tobin, T.G. Cotter, Prion protein fragment PrP-(106–126) induces apoptosis via mitochondrial disruption in human neuronal SH-SY5Y cells, *J. Biol. Chem.* 276 (2001) 43516–43523.
- [19] E. Paitel, C. Alves da Costa, D. Vilette, J. Grassi, F. Checler, Overexpression of PrPc triggers caspase 3 activation: potentiation by proteasome inhibitors and blockade by anti-PrP antibodies, *J. Neurochem.* 83 (2002) 1208–1214.
- [20] E. Paitel, R. Fahraeus, F. Checler, Cellular prion protein sensitizes neurons to apoptotic stimuli through Mdm2-regulated and p53-dependent caspase 3-like activation, *J. Biol. Chem.* 278 (2003) 10061–10066.
- [21] V. Perrier, K. Kaneko, J. Safar, J. Vergara, P. Tremblay, S.J. DeArmond, F.E. Cohen, S.B. Prusiner, A.C. Wallace, Dominant-negative inhibition of prion replication in transgenic mice, *Proc. Natl. Acad. Sci. U.S.A.* 99 (2002) 13079–13084.
- [22] T. Pillot, B. Drouet, M. Pincon-Raymond, J. Vandekerckhove, M. Rosseneu, J. Chambaz, A nonfibrillar form of the fusogenic prion protein fragment [118–135] induces apoptotic cell death in rat cortical neurons, *J. Neurochem.* 75 (2000) 2298–2308.
- [23] R.K. Plemper, D.H. Wolf, Retrograde protein translocation: ERAD-ication of secretory proteins in health and disease, *Trends Biochem. Sci.* 24 (1999) 266–270.
- [24] S.B. Prusiner, Prions, *Proc. Natl. Acad. Sci. U.S.A.* 95 (1998) 13363–13383.
- [25] J. Schultz, A. Schwarz, S. Neidhold, M. Burwinkel, C. Riemer, D. Simon, M. Kopf, M. Otto, M. Baier, Role of interleukin-1 in prion disease-associated astrocyte activation, *Am. J. Pathol.* 165 (2004) 671–678.
- [26] L. Solfarosi, J.R. Criado, D.B. McGavern, S. Wirz, M. Sanchez-Alavez, S. Sugama, L.A. DeGiorgio, B.T. Volpe, E. Wiseman, G. Abalos, E. Masliah, D. Gilden, M.B. Oldstone, B. Conti, R.A. Williamson, Cross-linking cellular prion protein triggers neuronal apoptosis in vivo, *Science* 303 (2004) 1514–1516.
- [27] G.C. Telling, T. Haga, M. Torchia, P. Tremblay, S.J. DeArmond, S.B. Prusiner, Interactions between wild-type and mutant prion proteins modulate neurodegeneration in transgenic mice, *Genes Dev.* 10 (1996) 1736–1750.
- [28] D. Westaway, J. Cayetano-Canlas, D. Groth, D. Foster, S.-L. Yang, M. Torchia, G.A. Carlson, S.B. Prusiner, Degeneration of skeletal muscle, peripheral nerves, and the central nervous system in transgenic mice overexpressing wild-type prion proteins, *Cell* 76 (1994) 117–129.
- [29] Y. Yedidia, L. Horonchik, S. Tzaban, A. Yanai, A. Taraboulos, Proteasomes and ubiquitin are involved in the turnover of the wild-type prion protein, *EMBO J.* 20 (2001) 5383–5391.
- [30] G. Zanusso, R.B. Petersen, T. Jin, Y. Jing, R. Kanoush, S. Ferrari, P. Gambetti, N. Singh, Proteasomal degradation and N-terminal protease resistance of the codon 145 mutant prion protein, *J. Biol. Chem.* 274 (1999) 23396–23404.
- [31] H. Zhou, F. Cao, Z. Wang, Z.X. Yu, H.P. Nguyen, J. Evans, S.H. Li, X.J. Li, Huntingtin forms toxic NH₂-terminal fragment complexes that are promoted by the age-dependent decrease in proteasome activity, *J. Cell Biol.* 163 (2003) 109–118.



More than a 100-fold increase in immunoblot signals of laser-microdissected inclusion bodies with an excessive aggregation property by oligomeric actin interacting protein 2/ β -lactate dehydrogenase protein 2

Naomi S. Hachiya^a, Takuya Ohkubo^b, Yoshimichi Kozuka^c, Mineo Yamazaki^d, Osamu Mori^e, Hidehiro Mizusawa^b, Yuji Sakasegawa^f, Kiyotoshi Kaneko^{a,*}

^a *Second Department of Physiology, Tokyo Medical University, Shinjuku-ku, Tokyo 160-8402, Japan*

^b *Department of Neurology and Neurological Science, Graduate School of Medicine, Tokyo Medical and Dental University, Bunkyo-ku, Tokyo 113-0034, Japan*

^c *Ultrastructural Research, National Institute of Neuroscience, National Center of Neurology and Psychiatry, Kodaira, Tokyo 187-8502, Japan*

^d *Department of Neurology and Nephrology, Nippon Medical School, Bunkyo-ku, Tokyo 113-8602, Japan*

^e *Second Department of Pathology, Nippon Medical School, Bunkyo-ku, Tokyo 113-8602, Japan*

^f *Division of Prion Protein Biology, Department of Prion Protein Research, Graduate School of Medicine, Tohoku University, Aoba-ku, Sendai 980-8575, Japan*

Received 6 July 2005

Available online 26 September 2005

Abstract

We established a histobiochemical approach targeting micron-order inclusion bodies possessing extensive aggregation properties in situ by using a nonchemical denaturant (oligomeric actin interacting protein 2/ β -lactate dehydrogenase protein 2 [Aip2p/Dld2p]) with the combinatorial method of laser-microdissection and immunoblot analysis. As a model, pick bodies were chosen and laser-microdissected from three different brain regions of two patients with Pick's disease. Initially, 500 to 2000 pick bodies were applied onto SDS-PAGE gels after boiling in Laemmli's sample buffer according to established immunoblotting procedures; however, only faint signals were obtained. Following negative results with chemical denaturants or detergent, including 6 M guanidine hydrochloride, 8 M urea, and 2% SDS, the laser-microdissected pick bodies were pretreated with oligomeric Aip2p/Dld2p, which possesses robust protein unfolding activity under biological conditions. Strikingly, only one pick body was sufficient to illustrate an immunoblot signal, indicating that pretreatment with oligomeric Aip2p/Dld2p enhanced the immunoblot sensitivity by more than 100-fold. Pretreatment with oligomeric Aip2p/Dld2p also allowed us to quantify the total protein content of pick bodies. Thus, use of oligomeric Aip2p/Dld2p significantly contributed toward the acquisition of information pertaining to the molecular profile of proteins possessing an extensive aggregation property, particularly in small amounts.

© 2005 Elsevier Inc. All rights reserved.

Keywords: Oligomeric Aip2p/Dld2p; Protein conformation unfolding activity; Laser-microdissection; Inclusion bodies; Pick bodies; Phosphorylated tau

While immunohistochemical analysis has been widely used for the characterization of microstructures under various conditions and of disorders at a light microscopic level, immunoblot analysis has been indispensable in

the analysis of proteins at a macroscopic level [1]. Currently, no analytical methods equivalent to the immunoblot have been developed against targets for examination under the microscope, although the recent development of a laser-microdissection methodology allows us to manipulate microstructures at microscopic regions of interest in situ [2].

* Corresponding author. Fax: +81 3 3351 6544.

E-mail address: k-kaneko@tokyo-med.ac.jp (K. Kaneko).

Against this backdrop, we developed a novel combinatorial method that uses laser-microdissection and immunoblotting to allow the characterization of the molecular profile of proteins at microscopic regions of interest. As a model, we examined brain samples of Pick's disease, a type of progressive presenile dementia that affects brain function, eventually causing loss of verbal skills and problem-solving ability [3]. Pick's disease accounts for 5% of all dementias and is characterized neuropathologically by distinct tau-immunoreactive intraneuronal inclusions known as pick bodies [4]. Abnormally phosphorylated tau proteins were detected from total brain homogenates [4–6], but no investigation has been reported with isolated pick bodies to date.

Given limited sample availability and the absence of in vitro amplification steps for proteins, use of laser-microdissected samples depends largely on highly sensitive protein detection methods [7]. Furthermore, these inclusion bodies generally possess extensive aggregation properties that often negatively affect the immunoblot assay. Unfortunately, use of conventional procedures, including sample pretreatment with chemical denaturing agents or detergent, was ineffective. In an effort to overcome the problem, oligomeric actin interacting protein 2 (Aip2p)¹ [8]/D-lactate dehydrogenase protein 2 (Dld2p) [9,10] was used as a non-chemical denaturant [11–13]. Dld2p [9,10] was initially identified as Aip2p using a two-hybrid screen to search for proteins that interact with actin [8]. During our search for protein conformation unfolding activity, we further identified oligomeric Aip2p/Dld2p isolated from *Saccharomyces cerevisiae* as exhibiting robust protein conformation unfolding activity [11]. Oligomeric Aip2p/Dld2p possesses a unique grapple-like structure with an ATP-dependent opening that is required for protein conformation unfolding activity [12,13]. In the presence of 1 mM ATP or AMP-PNP, oligomeric Aip2p/Dld2p bound to all substrates so far examined and subsequently modified the protein conformation. Furthermore, oligomeric Aip2p/Dld2p was able to modify the conformation of pathogenic highly aggregated polypeptides such as recombinant prion protein (rPrP) in the beta form, alpha-synuclein, and Aβ(1–42) in the presence of ATP in vitro [13]. This procedure consists simply of combining oligomeric Aip2p/Dld2p and 1 mM ATP in a reaction tube containing the collected pick bodies and then incubating the sample for 60 min at 30 °C.

Oligomeric Aip2p/Dld2p significantly increases the immunoblot signals by more than 100-fold. The histobiochemical approach detailed in this study allows us to analyze single pick bodies in the order of several micrometers in radius.

Materials and methods

After informed consent had been obtained, frontal (Y337F and Y332F) and temporal (Y332T) cortices from two patients with sporadic Pick's disease (patient 1 (Y337): female, 71 years old; patient 2 (Y332): male, 72 years old) were placed in a deep freezer (–80 °C) at Nippon Medical School until use. The procedures followed were in accordance with the institutional ethical standards on human experimentation.

Oligomeric Aip2p/Dld2p was expressed and purified as described previously [11,12]. Anti-tau AT8 (phosphorylation-dependent monoclonal antibody specific to phosphorylated Ser202/Thr205) and AT100 (specific to phosphorylated Thr212/Ser214) were purchased from Innogenetics. Anti-Aip2p/Dld2p antibody was raised against the synthetic peptide corresponding to the C-terminal 15 amino acid residues of Aip2p (VHYDPNGILNPYKYI) that were coupled through a COOH-terminal cysteine residue to bovine serum albumin (BSA) [11].

Slide preparations were made using a NexES Automated Immunohistochemistry Staining System (Ventana Medical Systems) with 1:200 AT8. Immunostained pick bodies (10–15 μm in diameter) (Table 1) were dissected using a Laser Microdissection System (Olympus Optical) coupled to a Hoya laser cutter (HCL2100, 30 mJ/pulse, 266 nm). Dissected samples were collected using a Cell Tram Oil hydraulic manual microinjector (Eppendorf) with distilled water.

Immunoblot analyses were performed as follows. First, total brain homogenates (10–40 μg) or laser-dissected pick bodies (500 pieces) were solubilized in 500 μl of ice-cold extraction buffer (Tris–chloride [pH 7.4], 0.8 M NaCl, 1 mM ethyleneglycotetraacetic acid [EGTA], 10% sucrose, and 1/1000 [w/v] protease inhibitor cocktail [Sigma] with 1% sodium *N*-lauroyl sarcosinate [sarkosyl]). Sarkosyl-insoluble fractions were collected by centrifugation at 182,000g for 30 min at 4 °C and then suspended in 50 mM Tris–chloride (pH 7.4). Samples were pretreated with 8 M urea (Wako Chemicals), 6 M guanidine hydrochloride (Nacalai Tesque), or 2% SDS (Wako Chemicals), followed by trichloroacetic acid (TCA) precipitation in an effort to denature or untangle the samples. Pretreatment with Aip2p/Dld2p was performed as described previously

Table 1
Quantitative analyses of pick bodies

	Y332T	Y332F	Y337F
Total protein (ng/pick body)	0.8	1.1	2.8
Average diameter (μm)	10	10	15
SRelative density	1.6	2.2	1.6

Note. The protein concentration of sarkosyl-insoluble fractions was measured following pretreatment with oligomeric Aip2p/Dld2p, and the relative density of the pick bodies was calculated. Frontal (Y337F and Y332F) and temporal (Y332T) cortices from two patients with sporadic Pick's disease (patient 1 (Y337): female, 71 years old; patient 2 (Y332): male, 72 years old) were analyzed.

¹ *Abbreviations used:* Aip2p, actin interacting protein 2; Dld2p, D-lactate dehydrogenase protein 2; rPrP, recombinant prion protein; BSA, bovine serum albumin; EGTA, ethyleneglycotetraacetic acid; TCA, trichloroacetic acid; PBS, phosphate-buffered saline; PBS-T, PBS containing 0.05% Tween 20; TBH, total brain homogenate; LC-MS/MS, liquid chromatography–tandem mass spectrometry.

[11–13]. Briefly, 1 to 500 ng of oligomeric Aip2p/Dld2p was mixed with the sarkosyl-insoluble fraction of 1 to 500 pick bodies at a ratio of 1 ng per 1 pick body in the presence of 1 mM ATP for 60 min at 30 °C in a total volume of 20 μ l. Samples were then loaded onto 12% SDS-PAGE gels and transferred onto 0.22- μ m nitrocellulose membranes in 25 mM Tris–190 mM glycine–0.01% SDS–20% methanol at 400 mA for 40 min at 4 °C. Membranes were blocked using 4% BSA in phosphate-buffered saline (PBS) containing 0.05% Tween 20 (PBS-T), incubated with 1:1000 (unless otherwise indicated) AT8 and AT100 in PBS-T overnight at 4 °C, washed with PBS-T several times at room temperature, and then incubated with 1:10,000 horseradish peroxidase-conjugated anti-mouse IgG antibody (Amersham) in PBS-T for 1 h at room temperature. After washing the membranes, the immunodecorated bands were visualized using ECL-plus (Amersham) and then analyzed using a Fluor-S MAX MultiImager or VersaDoc (Bio-Rad Laboratories).

The protein concentration of the pick bodies pretreated with oligomeric Aip2p/Dld2p was measured using a spectrophotometer (Tecan) at 595 nm in combination with a Protein Assay System (Bio-Rad Laboratories) according to the manufacturers' instructions. Oligomeric Aip2p/

Dld2p was applied at a ratio of 1 ng per 1 pick body, and the value was subtracted afterward.

Results

The laser-microdissection system combined with the sample collector facilitated the dissection of targets (Fig. 1A). Up to 500 pick bodies were collected each time over a period of 1 day. Initially, 500 pick bodies were applied onto SDS-PAGE gels after boiling in Laemmli's sample buffer according to established immunoblotting procedures [1]. However, only faint and blurred signals were obtained with anti-tau antibodies AT8 and AT100 (Fig. 1B, lane 4) in comparison with 10 to 40 μ g of total brain homogenate (TBH, Fig. 1B, lanes 2 and 3). Immunostaining of the entire gel, including the loading wells and the stacking gel, revealed no additional immunoblot signals that may have arisen from the extensive aggregation property of the pick bodies. Further increases in the number of pick bodies applied (up to 2000) could not improve the signal intensity (data not shown).

The effect of chemical denaturants or detergent, including 6 M guanidine hydrochloride, 8 M urea, and 2% SDS,

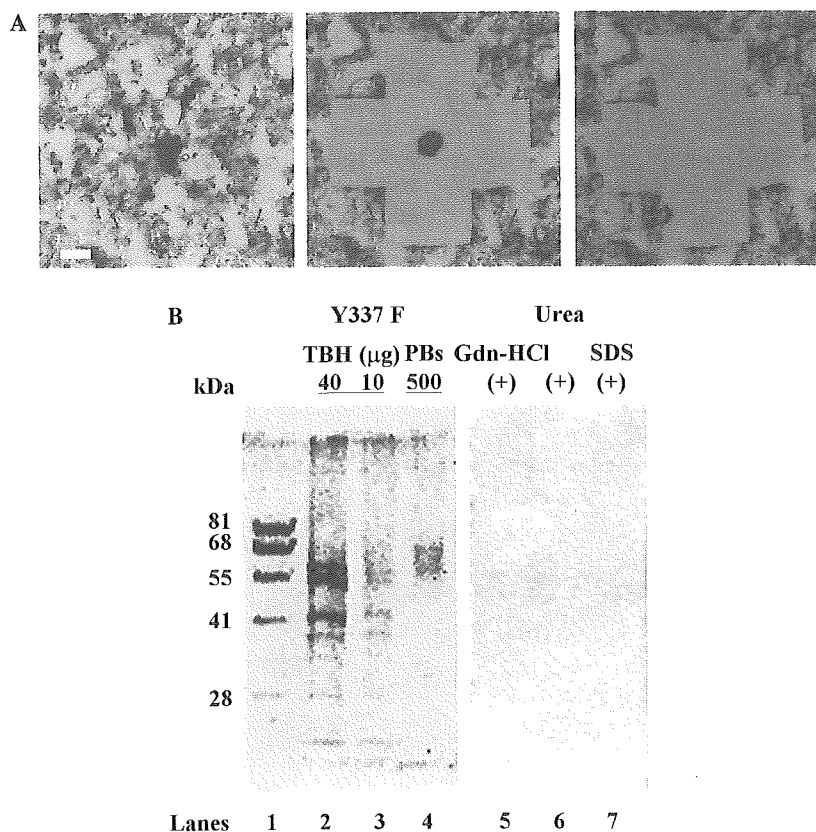


Fig. 1. Immunological analyses of laser-microdissected pick bodies (PBs). (A) Left panel: 5- μ m-thick cryosection. PBs of frontal cortex from patient Y337 (Y337F) are stained with AT8 (1:200, purple) and hematoxylin (blue). Middle and right panels: PBs isolated from the section using a laser-microdissector. Scale bar is 10 μ m. (For interpretation of the references to color in this figure legend, the reader is referred to the Web version of this article.) (B) Immunoblot analyses of PBs pretreated with chemical denaturants or detergent. Approximately 500 PBs were used for each trial. Lane 1: molecular weight marker (Dr. Western, Oriental Yeast); lanes 2 and 3: total brain homogenate (TBH) of Y337F (40 and 10 μ g, respectively); lanes 4 to 7: 500 laser-microdissected PBs of Y337F with no pretreatment (lane 4), 6 M guanidine hydrochloride (Gdn-HCl, lane 5), 8 M urea (lane 6), and 2% SDS pretreatment (lane 7). Samples were stained with anti-tau AT8 (1:1000) and AT100 (1:1000).